Investigation of Discharge Arc Phenomena in Ablative PPT

IEPC-2015-79／ISTS-2015-b-79

Presented at Joint Conference of 30th International Symposium on Space Technology and Science,
34th International Electric Propulsion Conference and 6th Nano-satellite Symposium
Hyogo-Kobe, Japan
July 4–10, 2015

Tony Schönherr,* Marcus Stein† and Kimiya Komurasaki‡
The University of Tokyo, Bunkyo, Tokyo, 113-8656, Japan

and

Georg Herdrich§
University of Stuttgart, Stuttgart, Baden-Württemberg, 70569, Germany

Pulsed plasma thrusters (PPT) transform electric energy into kinetic energy of an exhaust medium by means of a pulsed discharge. Due to the short discharge time, the nature of the discharge remained unraveled for long time. This study applies optical methods including high-speed camera observation and emission spectroscopy to describe the discharge arc in a pulsed plasma thruster in detail. Results include the position and width of the arc as a function of time and voltage as well as a description of the species based on the spectral data. Further, by using an analytical method to derive the temperature by the emission profile, a temperature distribution in the discharge area is derived and discussed.

Nomenclature

A	= emission probability
c	= ion concentration
E	= energy of atomic state
g	= degeneracy of atomic state
m	= electron mass
n	= number density
p	= pressure
T	= excitation temperature
x	= axis parallel to the direction of particle exhaust
z	= axis parallel to the direction pointing from anode to cathode
ε	= emission
λ	= wavelength
ν	= line wave frequency

*Assistant Professor, Department of Aeronautics and Astronautics, schoenherr@al.t.u-tokyo.ac.jp.
†Graduate Student, Department of Aeronautics and Astronautics, now with Karlsruhe Institute of Technology, Institute of Technical Thermodynamics, marcus.stein@kit.edu.
‡Professor, Department of Aeronautics and Astronautics, komurasaki@al.t.u-tokyo.ac.jp.
§Head of Plasma Wind Tunnel and Electric Propulsion, Institute of Space Systems, herdrich@irs.uni-stuttgart.de

I. Introduction

In a pulsed plasma thruster, electrical energy stored in a capacitive device is discharged between two electrodes, thereby ionizing the propellant, and accelerating the resulting particle plasma. However, differences prevail due to the variations in geometric design (coaxial or parallel electrode design), propellant (solid, liquid, gaseous) and so on.

A major observed difference concerns the passage of discharge current through the medium between the electrodes. Resulting from extensive work on gas-fed PPT (GPPT) at Princeton University[1], it was concluded that the discharge current is pinched into a current sheet, canted due to the Hall effect, and propagated at velocities exceeding 10 km/s. When investigating ablative PPT, however, a propagating current sheet was not observed by high-speed photography[2–4], emission spectroscopy[5], interferometry[5,6] or induction probes[2,6,7]. Instead, the results indicated that the main discharge current stays close to the propellant surface in form of a diffuse discharge arc, and that the ionized particles are moved and ejected as a result of the electromagnetic and the slighter electrothermal forces. In this present work, further optical diagnostic experiments are conducted to provide detailed insight into the phenomena concerning the discharge arc in ablative PPT. To do so, high-speed camera measurements and optical emission spectroscopy along the axis of acceleration are conducted with focus on the area close to the propellant ablation surface rather than the plasma plume.

From modeling research on the ablation itself, it was concluded that the ablation is not an instantaneous event as assumed in the early days of PPT research[8], but a rather continuous process that parallels with the discharge of electrical power[9–13]. Indications to support this assumption were found in experiments[5,14]. However, the question remains how the ablated material (in most cases: C_2F_4) is further decomposed to eventually form the plasma that is accelerated. It is known from emission spectroscopy of the plume that a variety of species exist[2,5,15] and that they appear at different timings throughout the discharge[16,17]. This study focuses on the creation and movement of the different species as derivable from the above-mentioned experiments. As is known that the emission is linked to temperature, a analytical method is used to derive the profile of excitation temperature from the ablation surface towards the plasma plume. The results are used to discuss the energy transfer between discharge energy and plasma.

II. Experimental

A. Thruster and Vacuum Environment

For this study, the PPT ADD SIMP-LEX is used that operates on solid PTFE as propellant and was used in previous studies[17]. It comprises of four 20 µF capacitors with a maximum rated voltage of 1300 V, and copper electrodes that are 20 mm apart at the propellant location. The electrodes are tapered and diverge towards the their tip[18]. A breech-fed configuration of the propellant is used to allow for visual access to the phenomena occurring close to the propellant surface.

The thruster is placed in a stainless steel vacuum chamber with 0.5 m in diameter, and 1 m in length that is pumped down by a two-stage vacuum pump system to an ultimate pressure of about 5×10^{-3} Pa prior to experiment.

B. Optical Setups

An Ultra-8 high-speed camera, capable of recording 8 pictures with 520x520 pixels, is used to detect the processes close to the propellant surface. Previous studies resulted in a choice of 20-100 ns as exposure time. Additionally, bandpass filters were used to observe certain species in the plasma with an FWHM of 10 nm. That is, the multitude of possible spectral lines does not permit to identify undoubtedly certain species. The camera is triggered by a pulse delay generator and synchronized with the ignition circuit of the thruster.

A SOL Instruments MS3504i Czerny-Turner monochromator spectrograph is used together with an iCCD camera to resolve the emission along the axis of exhaust from the propellant surface to about 10 mm from the surface. The spectral width of the image is 30 nm at 0.12 nm of spectral resolution (limited by spectrograph), which means that to cover the parts of the visible range interesting for this study, the central wavelength is frequently adjusted. A mercury-vapor lamp as well as a low-pressure cold cathode xenon lamp are used to calibrate the wavelength of the resulting two-dimensional images in the (x,λ)-plane whereas the x-position is calibrated by detecting a probe light laser.

III. Temperature Estimation

To derive a temperature profile from the emission spectra, a method proposed by Larenz[19] is used. This method considers that emission from a certain spectral line will be increasing as the excitation temperature increases, yet the density of the species will decrease with higher temperature as further ionization and excitation occurs. That is, every spectral line emission peaks at a characteristic temperature. Local thermal equilibrium and a negligible absorption are assumed in the derivation of equations. The two equations the method is based on are the line emission equation and the Saha equation:

$$\varepsilon = \frac{A}{4\pi} h\nu \frac{g_e}{g_i} \cdot n_i \cdot \exp^{-\frac{E_e}{kT}} \quad (1)$$

$$\frac{c^2}{1-c^2} \cdot p = \frac{(2\pi m)^{3/2}}{h^3} 2 \frac{g_j}{g_i} \cdot (kT)^{5/2} \exp^{-\frac{E_j}{kT}} \quad (2)$$

Therein, A refers to the emission probability, h to the Planck constant, g to the degeneracy, n to number density, m to the electron mass, E to the energy, k to the Boltzmann constant, p to the pressure, and T to the excitation temperature. The ion concentration c is defined by:

$$n_i = \frac{1-c}{1+c} \frac{p}{kT} \quad (3)$$

The indices i, e and j refer to the ground state, the excited state, and the ionized state respectively. Deriving Equation (1) by kT and combining with Equation (2), Larenz derived a transcendent equation for the temperature at maximum emission T^*:

$$\frac{h^3}{(2\pi m)^{3/2}} \cdot \frac{1}{2} \frac{g_i}{g_j} \frac{p}{E_j^{5/2}} \cdot \left(\frac{E_j}{kT^*}\right)^{5/2} \cdot \exp^{\frac{E_j}{kT^*}} = \left(\frac{\frac{E_j}{kT^*} + \frac{5}{2}}{\frac{E_a}{kT^*} - 1}\right)^2 - 1 \quad (4)$$

This means, that for any spectral emission line, there is a pressure-dependent characteristic temperature. Considering a single species in PTFE plasma, many spectral emission lines belong to each species, so depending on the line, the characteristic temperature will be slightly different. For an exemplary emission line of single-ionized carbon (657.805 nm), Figure 1 shows the normalized relative emission (Eq. (1) without line-specific constants normalized by its maximum value) at $p = 1$ bar as a function of excitation temperature with the effect of the Saha equation on n_i.

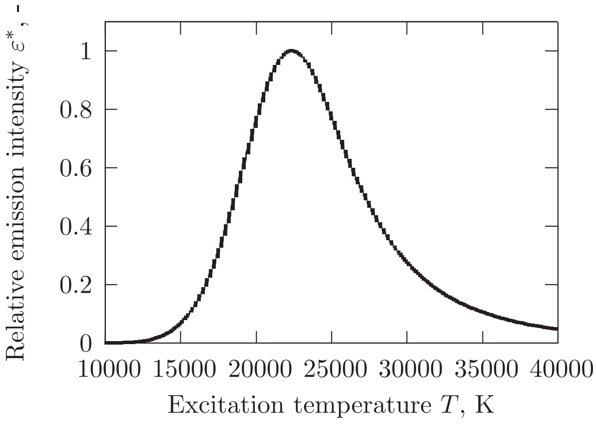

Figure 1. Spectral emission of C II (657.805 nm) at 1 bar.

The relative emission peaks at around 22400 K, which means that one could expect a plasma to be at that temperature if found that emission has its maximum there. This principle can be extended to the other species in PTFE plasma as well, and the relative emissions of some characteristic lines are shown in Figure 2. The characteristic wavelengths chosen here are strong lines found in PTFE emission spectra in previous studies[5], but the method works for all lines as long as spectral line info is provided. Note that Larenz pointed out that the calculation method for ions is slightly different than for atoms, but it was demonstrated that the resulting characteristic temperature varies insignificantly compared to the inaccuracy caused by the missing knowledge of actual pressure.

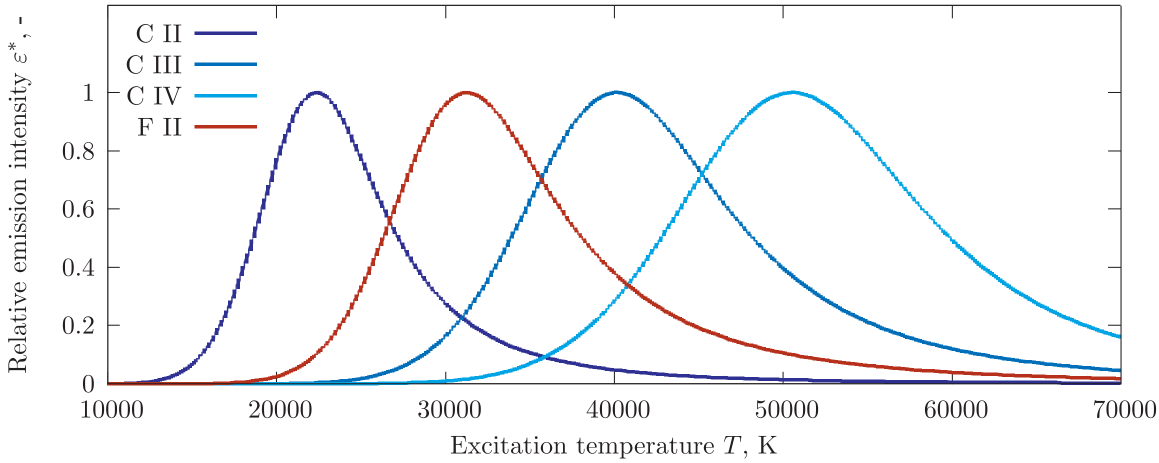

Figure 2. Relative spectral emission of expected common species in PTFE plasma at 1 bar. Respective wavelengths are 657.805 nm (C II), 464.742 nm (C III), 580.133 nm (C IV), and 402.473 nm (F II).

It is obvious that higher temperatures are needed for highly-ionized species, reflecting the intuitive expectation. Maximum emission of single-ionized fluorine is between single-ionized and double-ionized carbon as one would expect looking at the ionization potentials.

To investigate the influence of the pressure on the characteristic temperature, the values were calculated for all the emission lines in the investigated wavelength range for all possible species of PTFE plasma. The results are plotted in Figure 3 for a pressure range from 0 to 100 kPa. In previous research[5], a maximum pressure of about 30 kPa were derived in the plasma plume downstream of the discharge region. As this pressure is varying with time and space, it can only be assumed in this study that the pressure lies with the above-mentioned range. However, as the results show, the resulting characteristic temperature varies but little for a pressure beyond 10 kPa especially for the lower ionization levels. The influence of the pressure uncertainty will, hence, have less impact on the results of the temperature distribution evaluation than the inaccuracies in the emission spectroscopy.

The derived temperature results are used in the next chapter to derive the temperature distribution by combining them with the spectral emission maxima found by spectroscopy.

IV. Results and Discussion

A. Discharge phenomena

Ignition of the main discharge is triggered by the flashover discharge of a semiconductor igniter implemented in the nominal cathode. After discharge of the igniter, a delay of several microseconds precedes the main discharge, probably a result of the time it needs for the electrons to reach the nominal anode and form the discharge arc column. As a result of this delay, imaging of the very beginning of the main discharge is enabled. Exemplary VIS images of the supposed discharge arc are shown in Figure 4 in correlation with the voltage plot of main discharge, and igniter discharge.

During the initiation of the main discharge, emission of an arc column can be detected. The upper part of the arc is bent towards the igniter indicating an initial attachment of the arc between the anode and the positive igniter electrode. The image also indicates the presence of material capable of emitting light, either from the PTFE block or the electrodes. As the discharge proceeds, the cathode side of the arc recedes towards the propellant, and emission intensity grows with the increasing current in the arc. The arc remains at its position and in its shape during several microsecond into the discharge. As voltage and current decrease, the peak emission moves further downstream, eventually becoming diffuse indicating a disruption of the arc.

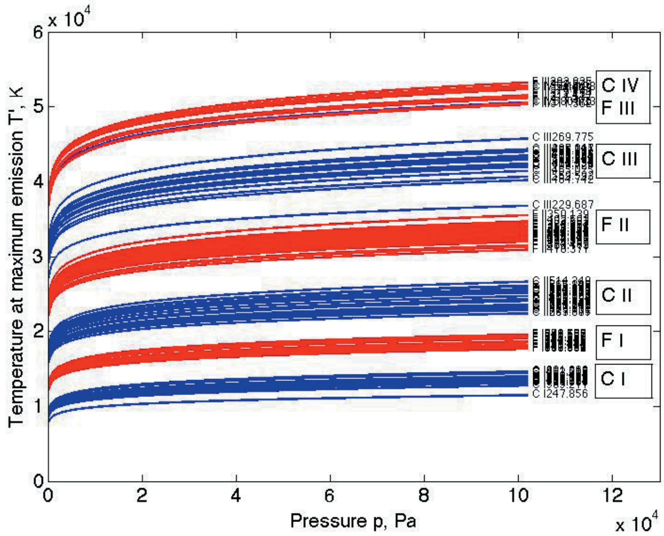

Figure 3. Pressure dependence of characteristic temperatures of spectral emission lines for various species found in PTFE plasma.

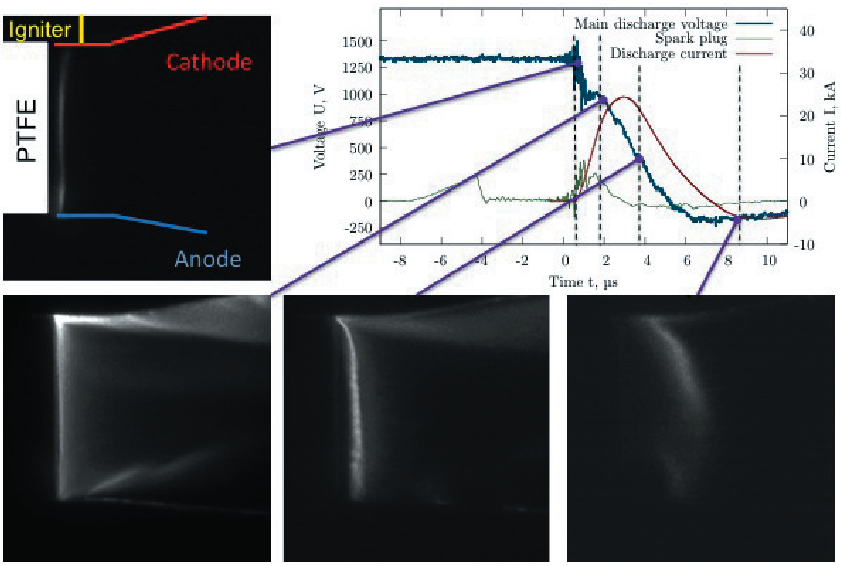

Figure 4. Exemplary images of the emission intensity in the visible range recorded by high-speed camera, and their respective discharge properties.

Images were processed and analyzed to derive the position of the discharge column and its width in x-direction (direction of exhaust). The results for the position are plotted in Figures 5(a) and 5(b). Three positions along the arc were evaluated; one close to each electrode, and one in the middle between them. An x-position of 0 mm indicates the surface of the solid PTFE propellant block.

Up to about 3 µs into the discharge for 900 V, and up to about 4 µs for 1300 V, the main intensity and, thus, the assumed discharge arc remains stationary. It is only after the decrease of discharge voltage that the arc starts moving away from the propellant surface. In Figure 5(b), it can further be seen how the arc recedes quickly at the cathode side during the first fraction of the discharge. This process is less obvious for higher discharge voltages. Nevertheless, one clearly observes a stable phase during the high-current part of the first discharge, whereas it is only when the discharge current substantially reduces, the arc structure appears to move out and break apart, although this might also be attributed to the decreasing current density and the

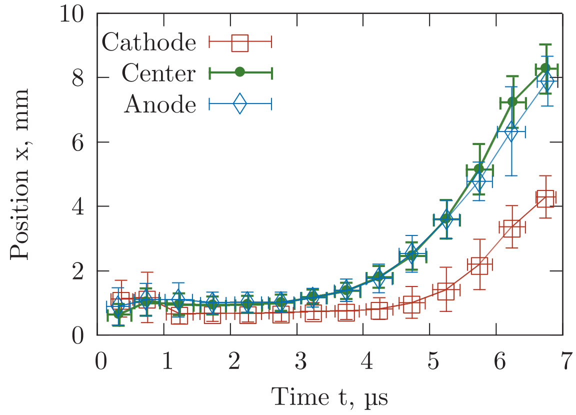

(a) Position of maximum emission at 1300 V of discharge voltage

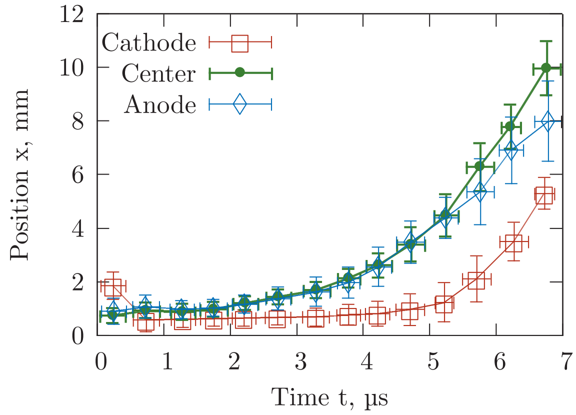

(b) Position of maximum emission at 900 V of discharge voltage

Figure 5. Time-dependent positions of emission maxima in the visible range as recorded by high-speed camera for different areas of the discharge zone. A position of 0 mm refers to the propellant surface.

related overall emission intensity.

The width of the discharge column was estimated by using an 80%-threshold of the maximum intensity. The resulting estimations for the arc width are plotted in Figure 6(a) for a discharge voltage of 1300 V, and in Figure 6(b) for 900 V respectively.

Similar tendencies as for the position can be seen with an almost constant width for the stable phase, and an increasing diffusiveness after 4 µs.

B. Behavior of plasma species

Application of bandpass filters revealed presence of certain species like C III almost exclusively in the expected high-current region whereas species like F II were found almost in the entire observed region defying a proper determination of the emission center as is exemplarily shown in Figures 7(a) and 7(b). However, for the higher ionized species, the overall intensity of the image was decreased, and the signal-to-noise ratio worsened for timings other than the peak current. Thus, analyses are more prone to errors for these species.

All reasonable images were analyzed for each respective filter, and exemplary results are plotted in Figure 8. The emission maxima for 4 filters are plotted for $t = 2.75$ µs at 1300 V of discharge voltage. The z-axis is defined as pointing from anode ($z = 0$ mm) towards cathode ($z = 20$ mm). The results show that the maxima for molecules and lower-energy ions are located closer to the propellant block as would be expected.

Plotting the results for the center axis against the discharge time, one obtains a similar image as for

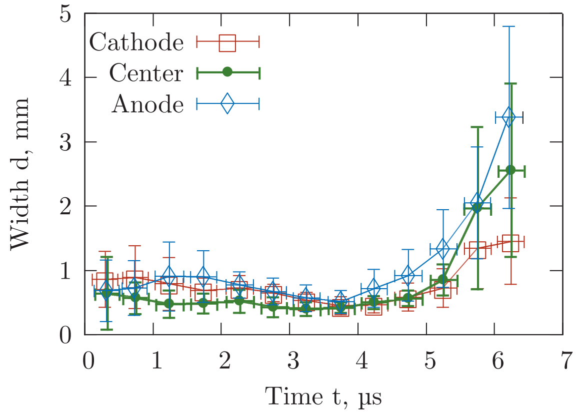

(a) Width of maximum emission at 1300 V of discharge voltage

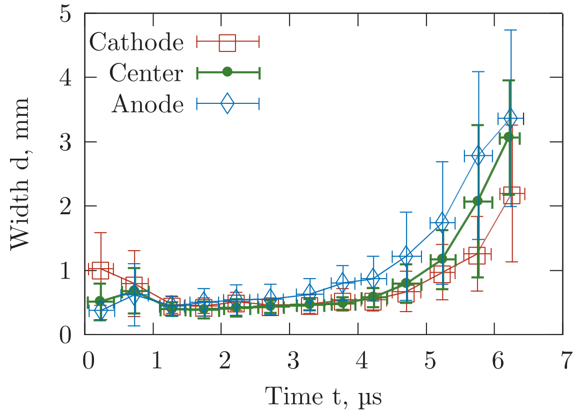

(b) Width of maximum emission at 900 V of discharge voltage

Figure 6. Time-dependent widths using a 80%-threshold of emission maxima in the visible range as recorded by high-speed camera for different areas of the discharge zone.

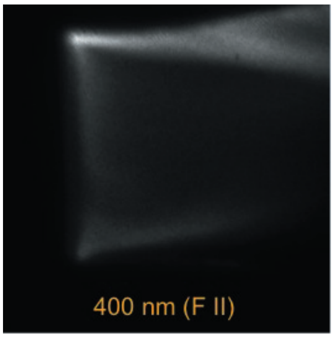

(a) Filtered image for 400 nm (strong expected emission from F II)

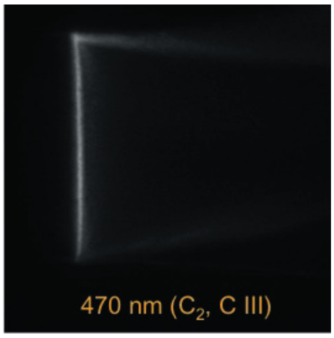

(b) Filtered image for 470 nm (strong expected emission from C III and likely C_2)

Figure 7. High-speed camera images using bandpass filters for different center wavelengths.

the full-range images in Figure 5. These results for 1300 V are plotted in Figure 9 for some selected filters. Again, the emission maxima fall in the order of the ionization potential, and as the maxima move further downstream, their relations to each other hardly change.

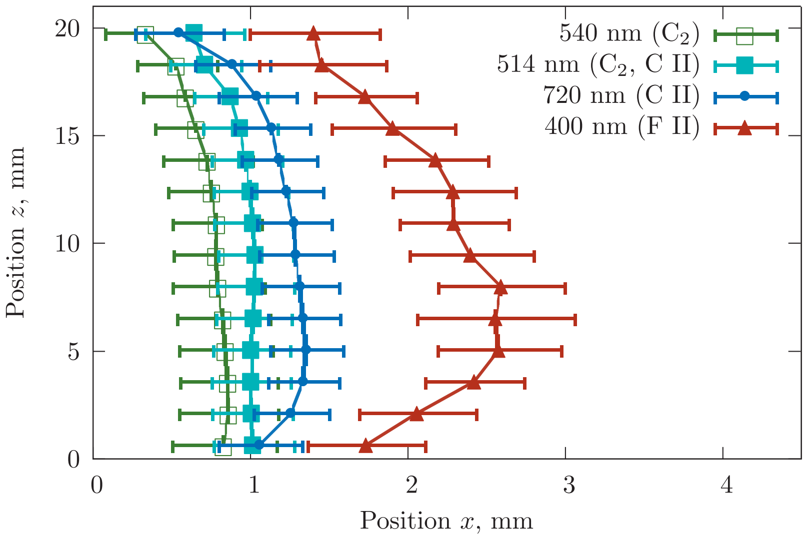

Figure 8. Emission maxima derived from high-speed camera images using various bandpass filters across the propellant surface for t = 2.75 µs.

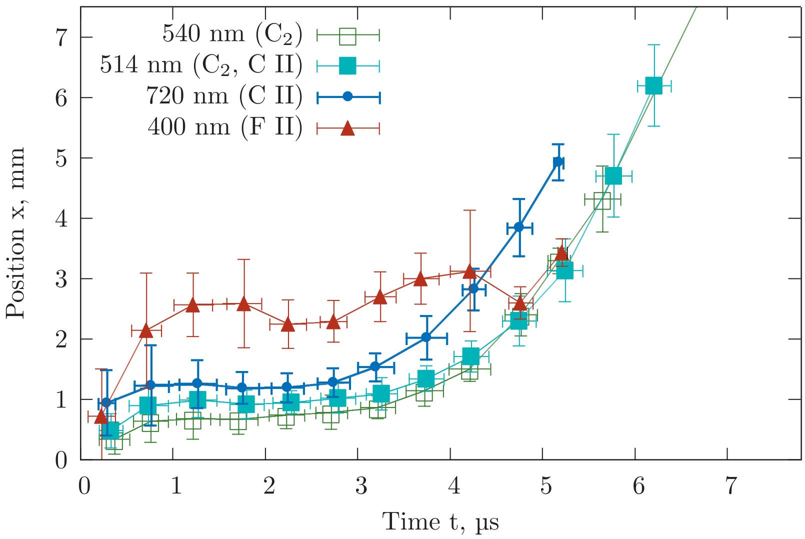

Figure 9. Emission maxima with variation in time derived from high-speed camera images on the center axis.

Emission spectroscopy along the x-axis yielded successfully results that could be evaluated. The spectrometer is capable of resolving 30 nm of wavelength range, and, thus, the experiments were conducted in ranges according to the filters used in the camera measurements for comparison. An exemplary spectrum is shown in Figure 10. The maxima of the individual lines are marked. It is obvious that lines from the same species have their peak intensity at the same position downstream.

Analysis of the spectra was conducted to evaluate the position of the emission maxima, and the width of the emission region respectively. This time, more species could be traced due to the distinctness of the lines. Exemplary results for 1300 V are shown in Figure 11.

The maxima fall into order according to the energy required for ionization. Similar tendencies are observed for positions close to cathode and anode, with the maxima close to the cathode located slightly further downstream.

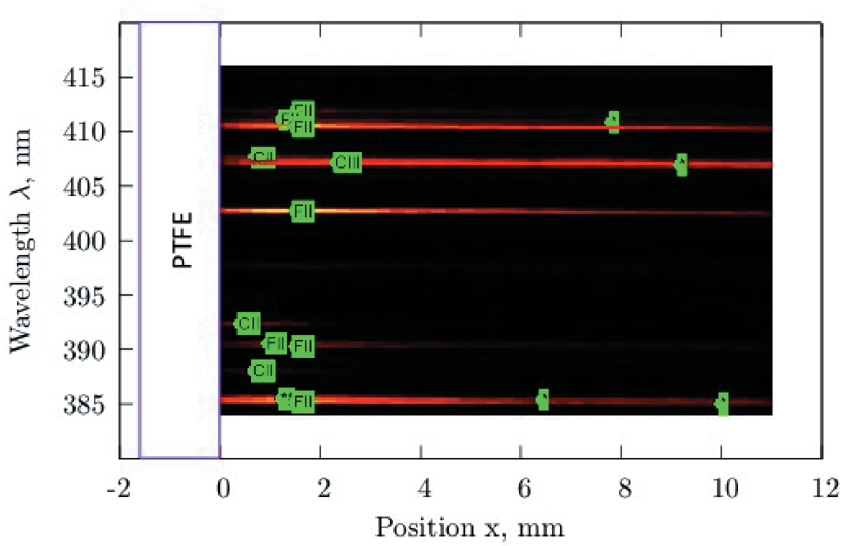

Figure 10. Exemplary emission spectrum with determined line maxima.

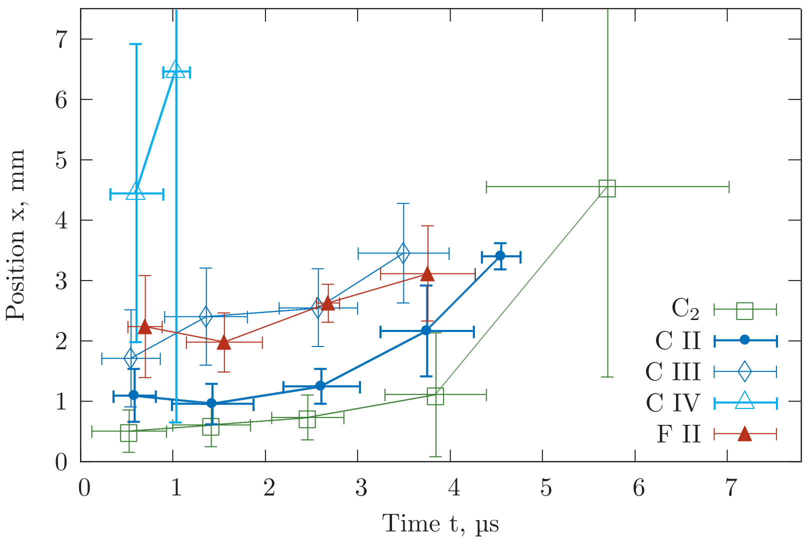

Figure 11. Emission maxima derived from optical emission spectroscopy averaged from various spectral lines for each species at 1300 V of discharge voltage.

It is worth noting that emission from any copper lines could not be observed. Given the similarity to vacuum arc processes, it was estimated that copper ejected from the cathode would show a high mean ion charge state[20]. This would lead to UV emissions far below the detectable range of the spectrometer used, and, hence, this study can neither confirm nor disprove the presence of highly ionized copper in the plasma.

Comparing the position of the emission maxima between individual species traced by emission spectroscopy (Figure 11) and their respective filter images (Figure 9) shows good agreement. In fact the difference lies within the error margin of one standard deviation. Comparing these results to the position of the full-range image (Figure 5(a)), one can see that the emission maxima (the proposed position of the discharge arc) fall between the maxima for C_2 and C II. This is especially interesting as $[C_2F_4]_n$ (PTFE) would yield twice as many fluorine ions as carbon. Further, C_2 was not detected further downstream in previous work[5] indicating full dissociation in the flow. It is, thus, to be expected that C_2 only appears in the transition between ablation (propellant surface) and dissociation/ionization (influence of high current section). Determination of the arc width by spectroscopy yielded similar results as for the camera measurements. However, due to different sensitivities in the sensors, and overlapping of spectral lines in the wavelength ranges of the bandpass filters, a direct comparison might be challenging.

The accordance of the results between full-range camera images, filtered images, and spectroscopic data is found to be independent of the discharge voltage, thereby supporting the conclusions about the general nature of the discharge.

C. Temperature Distribution

For the derivation of the temperature distribution, the results of the emission spectroscopy cannot be averaged as the characteristic temperature for each spectral line even of the same species is slightly different. This, of course, increases the susceptibility of the resulting distribution to uncertainties despite the growing number of data points. As the method proposed in Section III can only be applied to atomic and ionic species, one cannot use the method to the results of the C_2 molecule. With numerical modeling of the radiation, it might be possible to fit the spectral data to a certain temperature spectrum, but this exceeds the scope of this work. To be able to use the data nevertheless, a temperature of 5000 K is assumed. Combining the position of the emission maxima with the calculated characteristic temperatures, the distribution as shown in Figure 12 is derived.

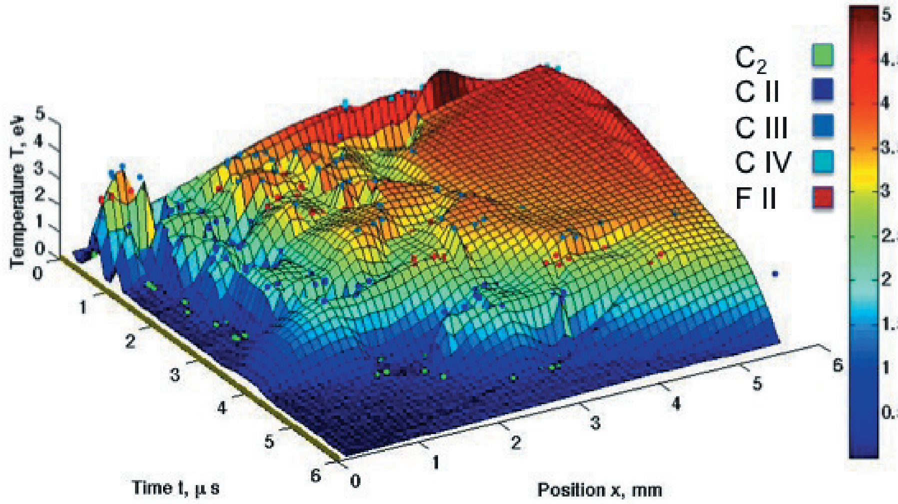

Figure 12. Derived temperature distribution in the 1300 V discharge on the center axis for an assumed pressure of 100 kPa.

Although the inaccuracies of the maxima position and the pressure-dependent temperatures exist, one can derive valuable information from the distribution. During the initial microsecond, the plasma is heated to its highest temperature within a short distance of 2-3 mm. This is likely due to the high power-to-mass ratio in the discharge creation as not enough material is yet ablated. As the discharge continues the temperature on average decreases, despite the discharge current increasing. Between 1 to 4 µs, the temperature profile along x remains mostly constant implying that the variation in discharge current (discharge power) affects more strongly the ablation processes rather than the ionization processes. As the current decreases further, the still hot ablation surface yields more material than could be properly heated and ionized, thus, reducing the overall temperature until the discharge polarity is reversed.

V. Conclusion

High-speed camera measurements and 1D emission spectroscopy were applied successfully for the first time to observe the discharge arc in a pulsed plasma thruster, and a temperature distribution profile for the discharge derived. Major findings include:

1. Three phases of arc behavior could be observed throughout the discharge: formation, maintaining (stable), and eventual disruption of the arc

2. Position and width of arc remain almost constant during the stable phase
3. Maxima of emission intensity occur for each species in order of energy necessary for creation
4. Good accordance between results of camera and spectroscopy (independent of discharge energy)
5. Temperature distribution indicates insufficient ablation during arc initiation, and insufficient ionization during disruption
6. Molecular C_2 detected close to propellant surface; no electrode material (Cu) observed

Acknowledgments

The authors want to thank Dr. K. Shimamura for assistance in the experimental work.

References

[1] Markusic, T. E., *Current Sheet Canting in Pulsed Electromagnetic Accelerators*, Ph.d. thesis, Princeton University, Princeton, NJ, USA, June 2002.

[2] Koizumi, H., Noji, R., Komurasaki, K., and Arakawa, Y., "Plasma Acceleration Processes in an Ablative Pulsed Plasma Thruster," *Physics of Plasmas*, Vol. 14, No. 3, March 2007, pp. 033506–1–10.

[3] Nawaz, A., Bauder, U., Böhrk, H., Herdrich, G., and Auweter-Kurtz, M., "Electrostatic Probe and Camera Measurements for Modeling the iMPD SIMP-LEX," 43rd AIAA/ASME/SAE/ASEE Joint Propulsion Conference, July 2007, AIAA-2007-5280.

[4] Schönherr, T., Komurasaki, K., Kawashima, R., Arakawa, Y., and Herdrich, G., "Evaluation of Discharge Behavior of the Pulsed Plasma Thruster SIMP-LEX," 46th AIAA/ASME/SAE/ASEE Joint Propulsion Conference, July 2010, AIAA-2010-6530.

[5] Schönherr, T., Nees, F., Arakawa, Y., Komurasaki, K., and Herdrich, G., "Characteristics of plasma properties in an ablative pulsed plasma thruster," *Physics of Plasmas*, Vol. 20, No. 3, March 2013, pp. 033503.

[6] Antropov, N. N., Diakonov, G. A., Orlov, M. M., Popov, G. A., Semenikhin, S. A., Tyutin, V. K., and Yakovlev, V. N., "Study of Physical Processes and Performance of Ablative Pulsed Plasma Thrusters," Space Propulsion, May 2010.

[7] Lau, M., Manna, S., Herdrich, G., Schönherr, T., and Komurasaki, K., "Investigation of the Plasma Current Density of a Pulsed Plasma Thruster," *Journal of Propulsion and Power*, Vol. 30, No. 6, Nov.-Dec. 2014, pp. 1459–1470.

[8] Jahn, R. G., *Physics of Electric Propulsion*, McGraw-Hill Book Company, Inc., New York, NY, USA, 1968.

[9] Keidar, M., Boyd, I. D., and Beilis, I. I., "On the model of Teflon ablation in an ablation-controlled discharge," *Journal of Physics D: Applied Physics*, Vol. 34, No. 11, June 2001, pp. 1675–1677.

[10] Gatsonis, N. A., Juric, D., and Stechmann, D. P., "Numerical Analysis of Teflon Ablation in Pulsed Plasma Thrusters," 43rd AIAA/ASME/SAE/ASEE Joint Propulsion Conference, July 2007, AIAA-2007-5227.

[11] Henrikson, E. M. and Mikellides, P. G., "Modeling of Ablation-Fed Pulsed Plasma Thruster Operation Using a New Approach to the Ablation Process," 44th AIAA/ASME/SAE/ASEE Joint Propulsion Conference, July 2008, AIAA-2008-4645.

[12] Kazeev, M. N. and Kozlov, V. F., "Ablation-Fed Discharge Characteristics," 31st International Electric Propulsion Conference, Sept. 2009, IEPC-2009-249.

[13] Schönherr, T., Zach, W. A., Komurasaki, K., Hörner, S., Arakawa, Y., and Herdrich, G., "Mechanical Probe and Modeling Efforts for Evaluation of Plasma Creation and Acceleration in PPT," 33rd International Electric Propulsion Conference, Oct. 2013, IEPC-2013-241.

[14] Scharlemann, C. A. and York, T. M., "Mass Flux Measurements in the Plume of a Pulsed Plasma Thruster," 42nd AIAA/ASME/SAE/ASEE Joint Propulsion Conference, July 2006, AIAA-2006-4856.

[15] Beiting, E. J., Qian, J., Russell, R. W., Pollard, J. E., Caven, W., and Corey, R., "Absolute Emission from the Mid-infrared to the Extreme Ultraviolet from a Pulsed Plasma Thruster (PPT)," 30th International Electric Propulsion Conference, Sept. 2007, IEPC-2007-268.

[16] Thomassen, K. I. and Vondra, R. J., "Exhaust Velocity Studies of a Solid Teflon Pulsed Plasma Thruster," *Journal of Spacecraft and Rockets*, Vol. 9, No. 1, Jan. 1972, pp. 61–64.
[17] Schönherr, T., Komurasaki, K., and Herdrich, G., "Propellant utilization efficiency in a pulsed plasma thruster," *Journal of Propulsion and Power*, Vol. 29, No. 6, Nov.-Dec. 2013, pp. 1478–1487.
[18] Schönherr, T., Nawaz, A., Herdrich, G., Röser, H.-P., and Auweter-Kurtz, M., "Influence of Electrode Shape on Performance of Pulsed Magnetoplasmadynamic Thruster SIMP-LEX," *Journal of Propulsion and Power*, Vol. 25, No. 2, March-April 2009, pp. 380–386.
[19] Larenz, R. W., "Über ein Verfahren zur Messung sehr hoher Temperaturen in nahezu durchlässigen Bogensäulen," *Zeitschrift für Physik*, Vol. 129, No. 3, May 1951, pp. 327–342.
[20] Shaw, P. V., *Pulsed Plasma Thrusters for Small Satellites*, Ph.d. thesis, University of Surrey, Guildford, UK, June 2011.